Nanovoid formation in helium-implanted single-crystal silicon studied by *in situ* techniques

S. Frabboni, F. Corni, C. Nobili, R. Tonini, and G. Ottaviani
Dipartimento di Fisica–Università di Modena e Reggio Emilia and INFM-National Research Center on nanoStructures and bioSystems at Surfaces-S3 Via G. Campi 213/A, 41100 Modena, Italy
(Received 28 July 2003; revised manuscript received 15 December 2003; published 22 April 2004)

In situ transmission electron microscopy and thermal desorption spectrometry have been employed to observe the evolution of vacancy-type extended defects and the corresponding helium state in helium implanted single crystal silicon during thermal ramp annealing. The structural evolution, starting with the formation of a platelike cluster of highly pressurized helium bubbles and ending in an empty nanovoid, is performed conserving the total volume of vacancy-type extended defects forming each cluster. Structural adjustments occur by surface diffusion inside each cluster following a migration and coalescence mechanism in presence of high pressure helium for $350\,^{\circ}\mathrm{C} < T < 570\,^{\circ}\mathrm{C}$. A conservative Ostwald ripening is observed for $570 < T < 700\,^{\circ}\mathrm{C}$ in presence of helium desorption.

DOI: 10.1103/PhysRevB.69.165209 PACS number(s): 61.72.Qq, 61.46.+w

INTRODUCTION

The thermal evolution of the damage associated with implantation of helium ions into crystalline silicon has been investigated either for the basic aspects concerning the defect production and the subsequent recovery or for the possibility of the process to modify the material and produce nanostructures.[1–5] The main features are associated to the very low transferred momentum during the helium-silicon collision which produces mostly localized Frenkel pairs, and to the very low solubility of helium in crystalline silicon which activates segregation and precipitation phenomena. Then an important role on the evolution of the damage during heat treatments is played by the mutual interactions of vacancy and interstitial type defects with the implanted specie in the presence of the constraint due to the crystal lattice. These interactions lead to the formation of peculiar defective structures, i.e., ''bubble,'' ''cavity,'' and ''void.'' Bubble refers to a nanometer sized, almost spherical hole and cavity refers to a hole having defined crystallographic facets; both kind of defects are believed to contain helium. On the contrary, void refers to an equilibrium, facetted, empty hole. These defects show typical contrast behavior in out-of-focus transmission electron microscopy (TEM) images that allow their recognition.[1,2,4,5]

Strong efforts have been recently done to understand the damage evolution in helium implanted silicon upon annealing. It has been demonstrated that void coarsening, observed in high temperature ($700 < T < 1000\,^{\circ}\mathrm{C}$) annealed samples, follows a migration and coalescence (MC) mechanism.[6] Thermal desorption spectrometry (TDS), being an *in situ* technique, has given quantitative information on helium state during the annealing on the basis of reasonable assumptions on helium-helium interaction and vacancy-type defect evolution.[5] On the contrary, the comprehension of the structural evolution and its correlation with helium content is still missing although it would represent an issue for a complete structural characterization of the Si(He) system. In fact *ex situ* TEM analyses carried out on low-temperature annealed samples ($200 < T < 700\,^{\circ}\mathrm{C}$), have shown the presence of a temperature-dependent, complex heterogeneity of helium-related vacancy-type extended defects,[5,7–9] but only speculative descriptions on their evolution have been reported.

The major problem encountered in modeling the system evolution from these data is the lack of experimental information concerning how the different structural variants transform each other to form a void and how helium atoms influence these structural changes. A deep knowledge on this evolution would be relevant not only from a fundamental point of view, but also for application fields where a control of size, distribution, and arrangements of voids are requested. In this paper we present results about the two main actors of the structural reaction, i.e., vacancy-type extended defects (studied by *in situ* TEM) and helium (detected by TDS) obtained *just during* nanovoid formation upon annealing under the same conditions, i.e., a thermal ramp.

EXPERIMENTAL

Single crystal [001] oriented Czochralski grown-silicon wafers have been implanted at the liquid nitrogen temperature with a dose of 1×10^{16} cm^{-2} of He^+ ions at an energy of 20 keV; this dose is slightly higher than the threshold ($\sim 8 \times 10^{15}$ ions/cm^2) for void formation after high temperature annealing. Plan view samples used for *in situ* TEM annealing experiments have been prepared by mechanical thinning and ion milling. Before the final thinning from the back side of the samples, approximately 50 nm of silicon have been milled from the surface by argon sputtering. This treatment has allowed us to obtain electron transparent areas completely embedding the damaged layer (centered at a depth of about 200 and 80 nm thick). The *in situ* TEM annealing experiments, from room temperature to $700\,^{\circ}\mathrm{C}$ at $2\,^{\circ}\mathrm{C}$/min, have been performed on a Philips CM30 TEM operating at 300 keV, using a GATAN 652 heating specimen holder. Images have been recorded on a GATAN 794 multiscan charged coupled device (CCD) camera using low dose illumination condition in order to minimize possible displacements of silicon atoms which could be induced by high angle, elastically scattered electrons. This is a small cross-section scattering process in silicon[10] whose effect, even for 300 keV electrons, can be reasonably excluded avoiding high

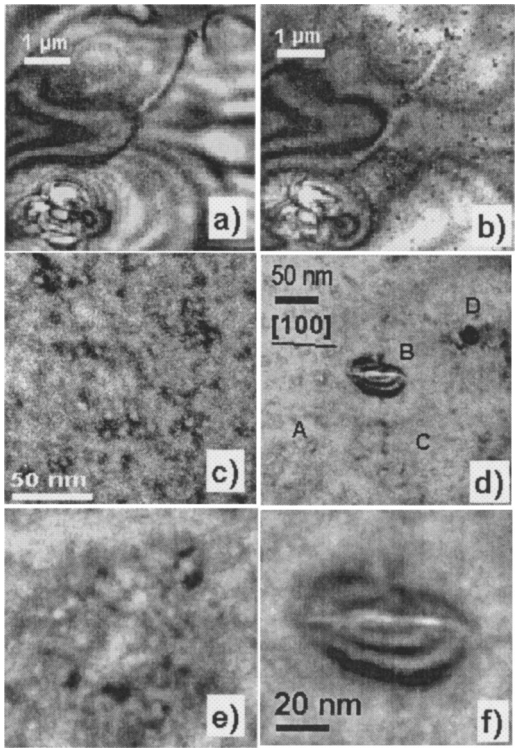

FIG. 1. (a) Image of the as-implanted sample: no bubbles are detected. (b) Image of the sample recorded at a temperature $T=250\,^{\circ}\mathrm{C}$: some strain centers are detected. (c) Bubbles and bubble clusters are observed at $T=300\,^{\circ}\mathrm{C}$. (d) Clusters are well defined at $T=350\,^{\circ}\mathrm{C}$. Clusters labeled A, C, D are (001) face on, whereas cluster B is (010) edge on. (e) High magnification image of cluster A showing its ''granular structure.'' (f) High magnification image of cluster B showing the discontinuous nature of the platelet forming the core.

current density irradiation. The effectiveness of both specimen preparation procedure and choice of the TEM illumination condition has been checked by comparing the defects observed in samples annealed in furnace with the ones observed in preliminary *in situ* experiments.

TDS measurements have been performed from room temperature to $700\,^{\circ}\mathrm{C}$ at $2\,^{\circ}\mathrm{C/min}$, at a pressure of about 10^{-4} Pa in operative conditions, while the sample has been heated by contact with a stainless-steel bar, whose controlled temperature has been monitored by a Chromel-Alumel thermocouple. Silver paint has been employed to ensure good thermal contacts between sample, thermocouple, and heater. The helium desorption has been evaluated by measuring the gas flux through the turbo-pump vacuum system (sample chamber volume 2×10^{3} cm^{3}, pumping speed for helium: $370l\ \mathrm{s}^{-1}$).

RESULTS AND DISCUSSION

The TEM image of the as implanted sample [Fig. 1(a)] does not show bubbles. *In situ* TEM annealing does not produce appreciable variation in the recorded images until a temperature of about $250\,^{\circ}\mathrm{C}$ is reached, Fig. 1(b), where strain contrast centers are detected. The image reported in Fig. 1(c) ($T=300\,^{\circ}\mathrm{C}$) shows that the contrast details are clusters of nanometric bubbles which are better defined after a further temperature increase [$T=350\,^{\circ}\mathrm{C}$, Fig. 1(d)]. This image shows that the clusters lie parallel to both (001) face-on plane (clusters labeled A, C, and D) and (010) [or (100)] edge-on planes (cluster labeled B). The presence in the same frame of (001) face-on and (010) edge-on clusters, showing at the end of the annealing process similar shape and surface area, will allow us to obtain a three-dimensional picture of their structural transformation. In particular images of cluster B will be considered the ''cross-section view'' of the face-on cluster A. Enlarged views of cluster A [Fig. 1(e)] and cluster B [Fig. 1(f)] show the internal structure of the clusters: the face-on view shows a tangle of bubbles and bubble aggregates of irregular shape; the edge-on view shows the ''core'' of the cluster formed by bubble aggregates having (010) mean habit plane and surrounded by a strong strain field evidenced by the elliptically shaped contrast fringes. Due to their aspect ratio and according to literature of *ex situ* experiments[5,7–9] the defects forming the core can be classified as ''platelets.'' By combining the structural information coming from Figs. 1(e) and 1(f) we can describe the three dimensional structure of the bubble cluster as formed by a multiplatelet core surrounded by a ''bubble atmosphere'' bonded to the cluster by the strong strain field produced by the cluster itself.

The field of view shown in Fig. 1(d) has been followed by TEM imaging during the overall experiment up to $700\,^{\circ}\mathrm{C}$; the relevant images are reported in Figs. 2, 3(a), and 4. In particular, Figs. 2(a) and 2(b) show two image sequences relative to the temperature-induced evolution of clusters A and B, respectively.

For $360<T<425\,^{\circ}\mathrm{C}$ a coarsening of the bubble aggregates forming the cluster is observed; this process produces a better definition of their shape [Fig. 2(a)]. The corresponding images in Fig. 2(b), show the increase of both the minor axis (hereafter called thickness) and the major axis (hereafter called length) of the platelets forming the core. This process appears due to the coalescence among platelets forming the core and bubble aggregates (having either platelet or bubble shape) surface connected with them [Fig. 2(b)]; consequently for $T=425\,^{\circ}\mathrm{C}$ the edge-on view of the cluster clearly shows a continuous core formed by a large single platelet [Fig. 2(b)]. A further temperature increase produces the progressive thickness increase of the platelet located near the center of the cluster [Fig. 2(b)] and the separation of the platelet with the small platelets and bubbles at the boundary [Fig. 2(a)]. For $T=455\,^{\circ}\mathrm{C}$ the cluster core is formed by highly an-isotropic cavities bounded by {100} and inclined facets [Fig. 2(b)] having their greatest axis along the two ⟨100⟩ directions of the (001) plane [Fig. 2(a)].

For $455<T\leqslant570\,^{\circ}\mathrm{C}$ a coalescence process between cavities located near the center of the cluster is observed [Fig. 2(a)]. When the cavities completely merge, then a planetary-like structure is formed[8,9] which is characterized by a single, large central cavity surrounded by a loop of small cavities. The corresponding images reported in Fig. 2(b) show the shape changes of the central cavity, performed by reducing the length and increasing both the thickness and the surface

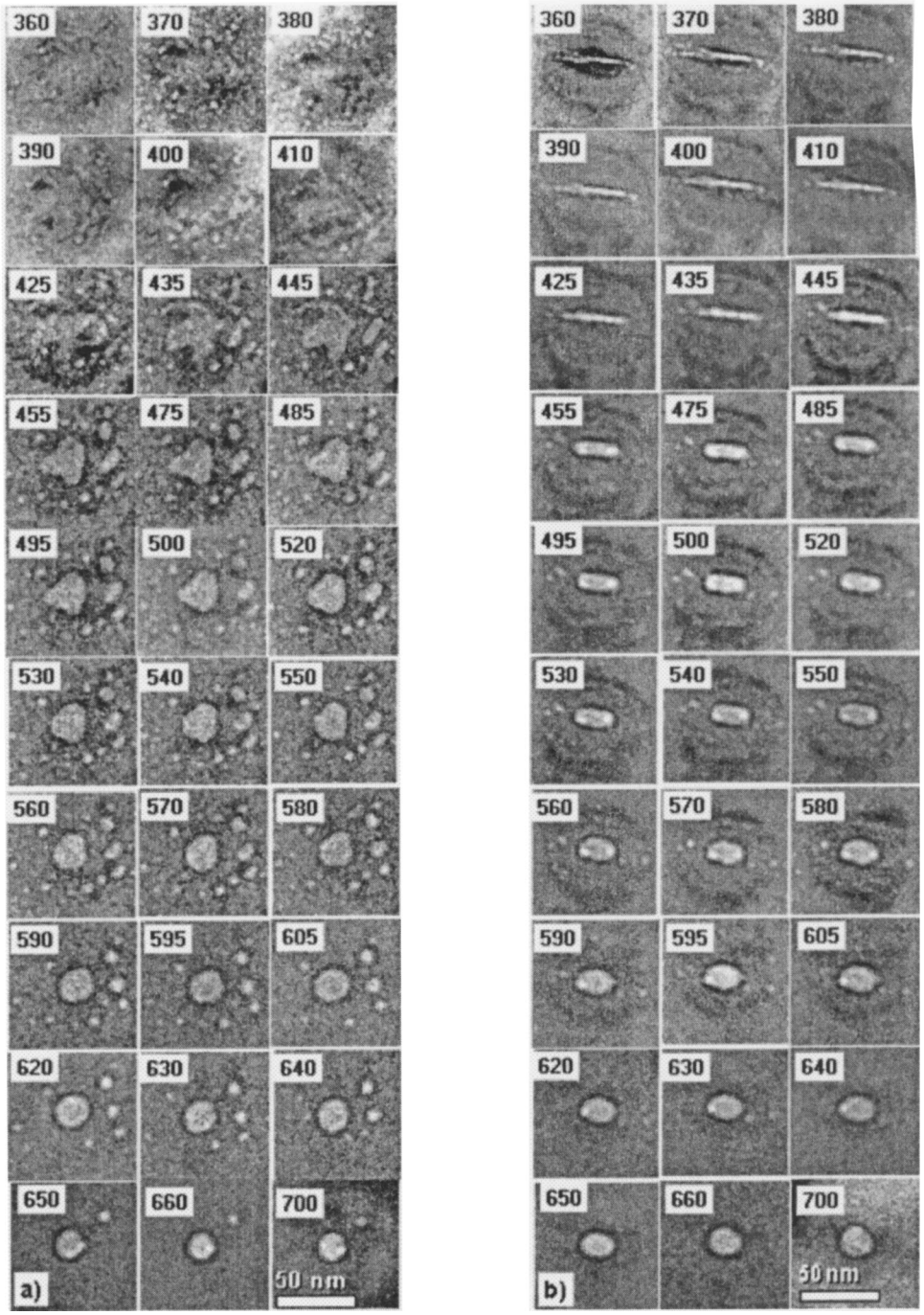

FIG. 2. Image sequences of a single bubble cluster taken in the temperature range $360 \leqslant T \leqslant 700\,^{\circ}\mathrm{C}$. (a) face-on cluster [labeled A in Fig. 1(d)]. (b) Edge-on cluster [labeled B in Fig. 1(d)]. The trace of the [100] direction is the same as in Fig. 1(d). The scale mark is the same for all figures. Labels on each picture indicates the temperature (°C) at which the image has been recorded. The structural modification path from a bubble cluster to a planetarylike cavity cluster and finally to a void is shown. The evolution of surface area of both the face-on and edge-on cluster can be measured directly from these sequence of images. Strain fringes surrounding the cluster are observed for $T < 650\,^{\circ}\mathrm{C}$.

area. An enlarged view of the edge-on cluster at $T = 570\,^{\circ}\mathrm{C}$ is shown in Fig. 3(a). This cavity is bounded by low-energy {100} and higher-energy inclined facets, thus suggesting that over-pressurized helium atoms are still trapped inside. The crystallographic trace analysis applied to this image suggests the presence of {113} facets; this suggestion has been confirmed by high resolution electron microscopy (HREM) imaging performed on [110] cross sections of samples annealed *ex situ* at 500 °C for 2 h [Fig. 3(b)]. These images have also shown that the small cavities forming the peripheral ring are generally bounded by low energy {111} and {100} facets.

From $T = 580\,^{\circ}\mathrm{C}$ up to the maximum temperature reached during the experiment (700 °C) the images reported in Fig. 2 show the continuous shrinkage of the small cavities and the corresponding shape changes of the central one, typical of an Ostwald ripening (OR) mechanism. In addition the contrast fringes observed in Fig. 2(b) show a progressive attenuation which can be ascribed to a strain relaxation phenomena. In fact at 700 °C the aspect ratio of the central cavity reaches an approximately unitary value corresponding to the lowest stress, lowest energy, equilibrium tetra-kaidechaedral shape typical of a void in silicon.[2] It is worth noting that the final values of the face-on and edge-on surface area are very close each other (270 vs 300 nm^2).

In Fig. 4 are reported some relevant images of the whole field of view recorded by the CCD camera during the *in situ*

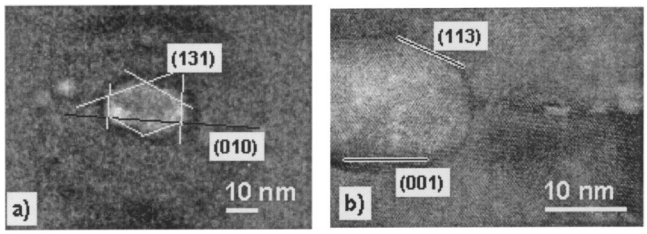

FIG. 3. (a) Enlargement of the image relative to the edge-on cluster B recorded at 570 °C. The trace on the sample surface of edge-on {100} (black and vertical white lines) and inclined {113} planes are reported. (b) High-resolution image obtained from a [110] cross section of a sample *ex situ* annealed at 500 °C for 2 h. In this image the trace of {001}, {113}, planes faceting the large cavities, and the {001} and {111} planes faceting the smaller ones can be observed edge on, thus uniquely identified.

experiment. From these images it is evident that the structural modifications producing a single void occur only inside each cluster, i.e., very short range diffusion is operative. In addition it is worth noting that, even though the presence of TEM sample surfaces could make the kinematics of the system evolution different from the one obtained by *ex situ* observations, nevertheless, due to the short range characteristic of the structural modification, it seems reasonable to assume that the observed phenomena are not dominated by the external surfaces. This implies that the evolution observed during *in situ* TEM analysis represent the structural features to be related to TDS experiments.

In order to correlate structural features with helium state inside the sample, quantitative data on total surface area of vacancy-type extended defects forming the face-on cluster, and core surface area of the edge-on cluster, obtained from Fig. 2, are reported in Fig. 5. The total surface area of the face-on cluster decreases with the temperature (from about 2400 to 270 nm^2); almost an opposite trend is found for the surface area of the edge-on cluster core. In addition, as each picture recorded during the thermal treatment shows both the face-on and the edge-on cluster, the total volume of vacancy-type extended defects of the cluster can be determined for each annealing step. Approximating the small bubbles having unresolved facets to sphere and larger platelet or voids to polyhedron of basis surface area and lateral surface area directly determined from Figs. 2(a) and 2(b), respectively, it is found that the total volume of the vacancy type defects of the cluster is conserved (approximately 6500 nm^3) during the structural evolution leading to the single void. This evidence strongly suggests that, after the volume increase of vacancy type extended defects observed during platelet formation (300–360 °C), the structural changes occur mainly by surface diffusion inside each cluster without additional interstitial ejection.

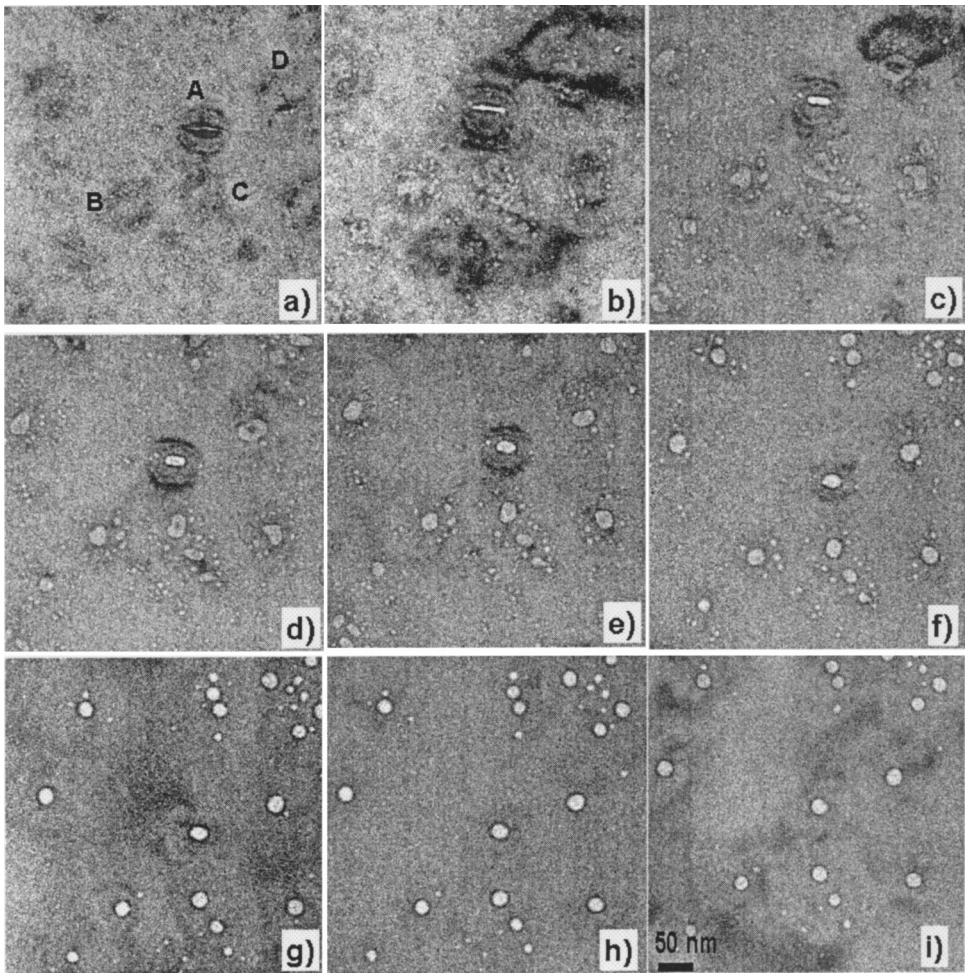

FIG. 4. Large field of view images of the *in situ* TEM experiments. Different clusters are visible, proving that the structural changes from platelet to void are confined inside a single cluster. (a) $T=360$ °C, (b) $T=435$ °C, (c) $T=475$ °C, (d) $T=540$ °C, (e) $T=570$ °C, (f) $T=605$ °C, (g) $T=650$ °C, (h) $T=660$ °C, (i) $T=700$ °C.

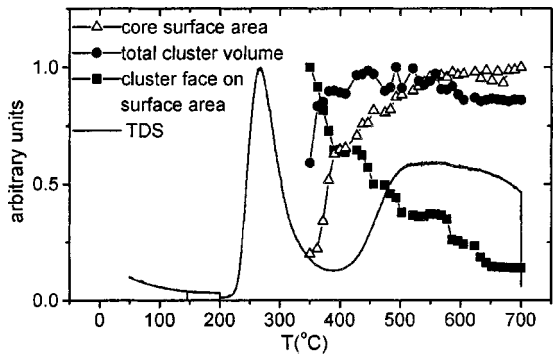

FIG. 5. Spectrum of helium effusion and quantitative data extracted from the TEM images reported in Fig. 2 (all the data are normalized to their maximum values). The first peak observed in TDS is not related to voids formation as it has been observed also in low dose samples where voids do not form. The total volume of vacancy-type extended defects forming the cluster (''cluster volume'') is conserved during the overall experiment.

We can then conclude that from a structural point of view the analysis of the evolution of a single cluster of vacancy type extended defects, shows a reaction path based on direct MC for $360<T\leqslant 570\,^{\circ}\mathrm{C}$ followed by a conservative OR at higher temperature when the largest cavity of the planetarylike cluster changes its shape increasing its volume at expense of the smaller ones by keeping constant the total volume of the vacancy type defects forming the cluster. This is the first direct experimental evidence of such phenomena in Si(He) system whose existence has been supposed in the literature.[8]

To correlate structural evolution and helium behavior, TDS experiments have been performed applying the same thermal ramp to the as implanted sample; the TDS spectrum is superimposed to the TEM data in Fig. 5. In the low-temperature range ($T<350\,^{\circ}\mathrm{C}$) a helium desorption peak is observed centered at $T=260\,^{\circ}\mathrm{C}$. It is generally accepted that this emission is not related to the phenomenon of voids formation since it has been observed even in very low dose samples containing only unstable vacancy clusters which anneal out with thermal treatment.[11] According to literature[11] this emission peak is ascribed to the helium release from the innermost helium distribution tail where the vacancy concentration produced by the ion implantation process is very low and a suitable ratio between vacancy and helium atoms concentration is not reached. During further temperature increase ($260<T<450\,^{\circ}\mathrm{C}$) helium desorption reaches a minimum. Comparison with *in situ* TEM images shows that the corresponding structural variant in crystalline silicon are the platelets, thus indicating that these defects are cracks opened by almost two dimensional helium precipitates stressing the silicon matrix. The pressure inside a platelet can be estimated of the order of 10 GPa according to literature[12] and assuming silicon shear modulus and Poisson's ratio equal to 64 and 0.28 GPa, respectively. This morphology is generally observed in second phase precipitation when the elastic contribution to the system free energy dominates with respect to the surface energy one. In the Si(He) system the source of the elastic energy is the high pressure exerted by the trapped helium atoms inside the platelet; the driving force for helium trapping is the energy gain, about 1 eV,[5,11] of the transformation from the solid solution phase to the precipitate phase.

The further heat supply induces the helium effusion from clusters represented by the large helium emission detected for $T>450\,^{\circ}\mathrm{C}$. The shape and the relatively low temperature of the emission peak is consistent with an heterogeneous distribution of bubbles and cavities containing highly pressurized helium [low pressure permeation occurs at least at $700\,^{\circ}\mathrm{C}$ (Ref. 11)]. These data are in agreement with the heterogeneous morphologies of vacancy-type extended defects observed inside each cluster. In particular, it seems safe to ascribe the emission in the temperature region $450\,^{\circ}\mathrm{C}<T<570\,^{\circ}\mathrm{C}$ to high pressure helium atoms trapped inside the small platelets or isolated bubbles which merge into the central part of the cluster to form planetarylike structures. The high-temperature emission ($T>570\,^{\circ}\mathrm{C}$) can be ascribed to helium atoms trapped inside the cavities of the planetarylike structures where the small cavities are emptied first, thus becoming unstable voids that annihilate into the larger one.

CONCLUSIONS

In conclusion in this paper the evolution from a cluster of helium bubbles to a single void *during annealing* has been reported, merging the structural changes and the helium behavior obtained by *in situ* techniques. It has been found that the void, the structural variant observed when helium is almost completely effused from the surface, is the final state of a structural reaction starting with the formation of a highly pressurized cluster of bubbles having a plateletlike core, whose adjustments are performed inside each cluster and conserving the total volume of vacancy-type defects of the cluster. For $360<T<570\,^{\circ}\mathrm{C}$, in presence of negligible helium effusion, by imaging of vacancy type extended defects it has been possible to observe the operating coarsening mechanism of the structural reaction which is MC by surface diffusion.

At higher temperature, when planetarylike clusters of cavities are formed, the structural modifications, which in this temperature range are associated to helium effusion, include both the dissolution of small cavities and the shape modification of the larger ones; a conservative OR inside each cluster seems to be operating. Shape changes are therefore determined by a balance between the elastic free energy stored in the matrix due to helium precipitation, which prefers platelet morphology, and surface free energy, which is minimized by spherical and faceted shape when helium is desorbed. Some of these results (role of the stress field in voids formation, constant reaction volume) represent important hints for future experiments aiming to control voids nucleation for their exploitation as template for buried nanostructure in silicon.

ACKNOWLEDGMENTS

The CNR-IMM Bologna section (formerly LAMEL) is acknowledged for TEM use.

[1] C.C. Griffionen, J.H. Evans, P.C. de Jong, and A.Van Veen, Nucl. Instrum. Methods Phys. Res. B **27**, 417 (1987).
[2] D.J. Eaglesham, A.E. White, L.C. Feldman, N. Moriya, and D.C. Jacobson, Phys. Rev. Lett. **70**, 1643 (1993).
[3] S.M. Myers, D.M. Follstaedt, H.J. Stain, and W.R. Wampler, Phys. Rev. B **47**, 13380 (1993).
[4] V. Raineri, P.G. Fallica, G. Percolla, A. Battaglia, M. Barbagallo, and S.U. Campisano, J. Appl. Phys. **78**, 3727 (1995).
[5] G.F. Cerofolini, F. Corni, S. Frabboni, C. Nobili, G. Ottaviani, and R. Tonini, Mater. Sci. Eng., R. **27**, 1 (2000).
[6] J.H. Evans, Nucl. Instrum. Methods Phys. Res. B **196**, 125 (2002).
[7] P.F.P. Fichtner, J.R. Kaschny, R.A. Yankov, A. Mücklich, U. Kreißig, and W. Skorupa, Appl. Phys. Lett. **70**, 732 (1997).
[8] P.F.P. Fichtner, J.R. Kaschny, M. Behar, R.A. Yankov, A. Mücklich, and W. Skorupa, Nucl. Instrum. Methods Phys. Res. B **148**, 329 (1999).
[9] F. Corni, G. Calzolari, F. Gambetta, C. Nobili, R. Tonini, and M. Zapparoli, Mater. Sci. Eng., B **71**, 207 (2000).
[10] L. Reimer, *Transmission Electron Microscopy, Springer Series in Optical Sciences*, 2nd ed. (Springer, Berlin, 1989).
[11] G.F. Cerofolini, G. Calzolari, F. Corni, S. Frabboni, C. Nobili, G. Ottaviani, and R. Tonini, Phys. Rev. B **61**, 10 183 (2000).
[12] J. Chen, P. Jung, and H. Trinkaus, Phys. Rev. Lett. **82**, 2709 (1999).